Cement and Concrete Research 41 (2011) 1001–1014

Contents lists available at ScienceDirect

Cement and Concrete Research

journal homepage: http://ees.elsevier.com/CEMCON/default.asp

The relation between fiber orientation and tensile behavior in an Ultra High Performance Fiber Reinforced Cementitious Composites (UHPFRCC)

Su-Tae Kang [a], Jin-Keun Kim [b,*]

[a] Structural Engineering & Bridges Research Division, Korea Institute of Construction Technology, 1190 Simindae-ro, Ilsanseo-gu, Goyang, 411-712, South Korea
[b] Department of Civil and Environmental Engineering, Korea Advanced Institute of Science and Technology (KAIST), 373-1 Guseong-dong, Yuseong-gu, Daejeon, 305-701, South Korea

ARTICLE INFO

Article history:
Received 16 August 2010
Accepted 31 May 2011

Keywords:
Tensile properties (C)
Composite (E)
Fiber reinforcement (E)
High performance concrete (E)
Orientation

ABSTRACT

In this study, the effect of the fiber orientation distribution on the tensile behavior of Ultra High Performance Fiber Reinforced Cementitious Composites (UHPFRCC) was investigated. The tensile behavior was explored separately in two stages; pre-cracking and post-cracking tensile behaviors. Pre-cracking tensile behavior is expressed using the mechanism of elastic shear transfer between the matrix and the fiber in the composites. Post-cracking tensile behavior was expressed as the combined behavior of the resistance by the fibers and the matrix, considering a probability density distribution for the fiber orientation distribution across crack surface and a pullout model of steel fiber. The effect of the fiber orientation distribution was found to be very small on pre-cracking behavior, but to be significant on post-cracking behavior of UHPFRCC. The predicted results were compared with the experimental results, and the comparison presented satisfactory agreement.

1. Introduction

Ultra High Performance Fiber Reinforced Cementitious Composites (UHPFRCC) dealt with in this study shows very high strength, self compacting ability, and high toughness. It does not contain coarse aggregates and develops compressive strength exceeding 150 MPa with improved toughness through mixing of 2 vol.% of steel fibers that are 13 mm long and 0.2 mm in diameter.

In general, the most important advantage of adopting Fiber Reinforced Concrete (FRC) is the increase of tensile strength and enhancement of toughness. In other words, fibers in FRC resist against crack propagation with the help of stress transfer from the matrix to the fibers. FRC thus exhibits strain hardening behavior after first cracking as well as improvement in energy absorption capacity and toughness.

In UHPFRCC, a steel-fiber reinforced cementitious composite, it is therefore clear that the improvement in tensile properties is achieved by adding steel fibers. In order to understand its tensile properties and the performance of structures using the composites clearly, research on the effect of fiber reinforcement should be first conducted.

To date, most researches on the effect of fiber reinforcement have been mainly focused on the effects of geometric shape, type, and volume fraction of fiber [1–9]. Although there have been also numerous studies regarding the effect of fiber distribution [10–14], they mostly were devoted to the correlation at a macro-structural level between fiber distribution characteristics (e.g. a coefficient to represent the average dispersion or orientation of fibers throughout the composites) and tensile properties (e.g. tensile strength or toughness). Few studies have adopted a systematic approach from a microscopic to macroscopic view; that is, from the bond behavior of individual fiber distributed in the composites to the tensile behavior of a fiber reinforced composite and its structural performance. While some researchers have focused on the systematic approach with special interest in the fiber orientation distribution [15,16], the approaches were limited to analytical studies with the assumption of an idealized fiber distribution. They did not consider the actual fiber distribution, which is affected by diverse factors such as placing method, form shape, and fiber geometry.

Meanwhile, recent researches on FRC unveiled that the rheology of the FRC mix plays an important role in fiber orientation and thus its mechanical performance [17–19]. Many researchers are getting more interest on the effect. In an effort to obtain better performance with better fiber orientation distribution, there has been a simple attempt to induce fiber alignment by extrusion forming process [20]. In another way, there have been efforts to investigate the variation of fiber orientation distribution with different fabrication processes and quantitatively estimate its effect on the mechanical performance, especially tensile behavior [21–23]. Wuest et al. [24] proposed a meso-mechanical model to predict the UHPFRCC tensile hardening response considering the effect of realistic fiber orientation distribution on it.

This study was intended to investigate the effect of the fiber orientation distribution on the tensile behavior of UHPFRCC, considering the pullout behavior of each fiber in the composites and the actual fiber

* Corresponding author. Tel.: +82 42 350 3614; fax: +82 42 350 3688.
E-mail address: kimjinkeun@kaist.ac.kr (J.-K. Kim).

0008-8846/$ – see front matter © 2011 Elsevier Ltd. All rights reserved.
doi:10.1016/j.cemconres.2011.05.009

distribution obtained from experimental specimen. The tensile behavior was explored separately in two stages, pre-cracking and post-cracking tensile behaviors.

2. Theoretical approach for tensile behavior

2.1. Pre-cracking tensile behavior

Before any cracking has taken place in the matrix, during the early stages of loading, the interaction between the fiber and the matrix is elastic in nature. The stress developed at the interface is a shear stress which is required to distribute the external load between the fibers and matrix, this elastic shear transfer is the major mechanism to be considered for predicting the pre-cracking tensile behavior of fiber reinforced composites. The elastic shear stress distribution along the fiber–matrix interface is non-uniform. The first analytical model to describe the stress transfer in the elastic zone was developed by Cox [25]. Later models were based on similar concepts; they differed only in some of their numerical parameters. These models are usually referred to as shear lag theories. Let us consider a steel fiber embedded in a matrix, subjected to tensile stress as shown in Fig. 1.

A schematic representation of the deformations around a fiber before and after loading is provided in Fig. 1(a), and the elastic shear stress distribution at the interface and the tensile stress distribution in the fiber are illustrated in Fig. 1(b). The stress field developed due to these deformations can be calculated with several simplifying assumptions. Cox [25] derived the following equations for the tensile stress, $\sigma_f(x)$, in the fiber, and the elastic shear stress at the interface, $\tau(x)$, at a distance x from the fiber end:

$$\sigma_f(x) = E_f\varepsilon_m\left\{\frac{1-\cosh\beta_1\left(\frac{l}{2}-x\right)}{\cosh\frac{\beta_1 l}{2}}\right\} \tag{1}$$

$$\tau(x) = E_f\varepsilon_m\left\{\frac{G_m}{2E_f\ln(R/r)}\right\}^{1/2}\frac{\sinh\beta_1\left(\frac{l}{2}-x\right)}{\cosh\frac{\beta_1 l}{2}} \tag{2}$$

where β_1 is expressed by Eq. (3).

$$\beta_1 = \left\{\frac{2G_m}{E_f r^2\ln(R/r)}\right\}^{1/2} \tag{3}$$

In Eq. (1), R represents the radius of the matrix around the fiber, r means the radius of the fiber, l is the length of the fiber, E_f is equal to the modulus of elasticity of the fiber, and G_m is the shear modulus of the matrix at the interface.

The value R/r depends upon the fiber packing and the fiber volume content of the composites. The following equations for long fibers of circular cross-section have been derived [27].

For square packing:

$$\ln(R/r) = \frac{1}{2}\ln\left(\pi/V_f\right) \tag{4}$$

For hexagonal packing:

$$\ln(R/r) = \frac{1}{2}\ln\left[2\pi/\left(3V_f\right)^{1/2}\right] \tag{5}$$

From Eqs. (1) to (3), the calculated shear stress distribution at the interface, and the tensile stress distribution in the fiber are presented in Fig. 1(b). The shear stress is maximum at the ends of the fiber and drops to zero at the center. It is in this end zone that the stress is transferred from the matrix to the fiber, gradually building up tensile stress within the fiber. The tensile stress increases from the fiber end moving inward, reaching a maximum at the center.

Laws [28] has indicated that in the elastic case, the contribution of the fiber, and thus its efficiency, is a function of the strain ε_c in the composites. For elastic stress transfer, the average stress in the fiber, $\overline{\sigma}_f$, as a function of ε_c is:

$$\overline{\sigma}_f = E_f\varepsilon_c\left(\frac{1-\tanh\beta_1 l/2}{\beta_1 l/2}\right) \tag{6}$$

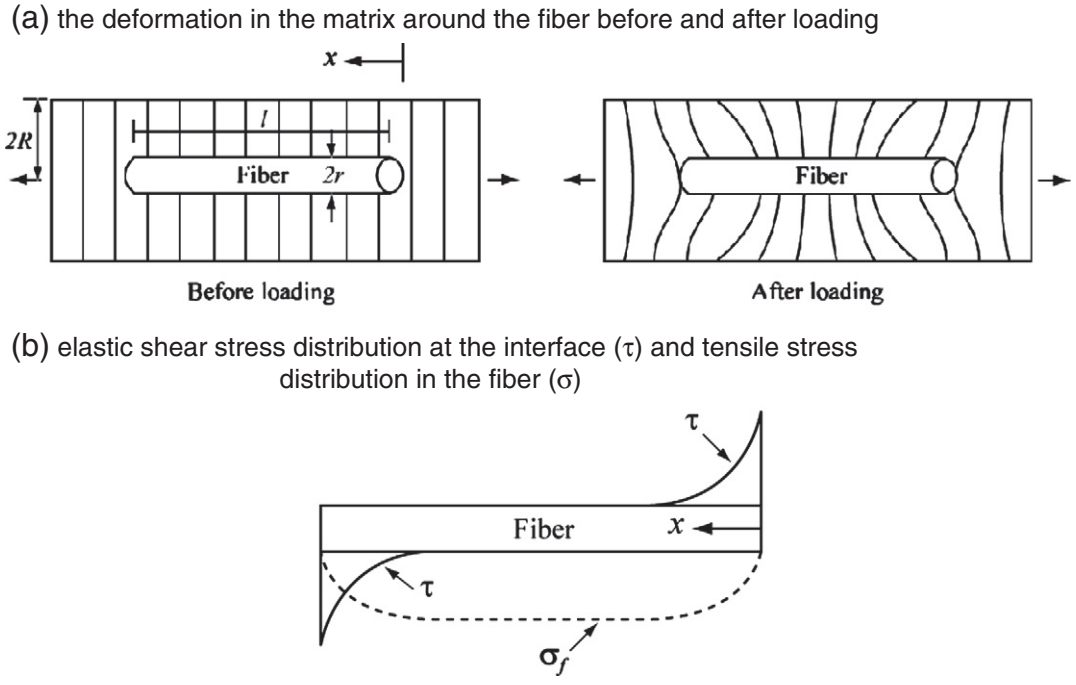

Fig. 1. Schematic description of a fiber embedded in a matrix, and the deformation and stress fields [26].

The tensile stress of the composites is calculated based on the rule of mixture, expressed by Eq. (7).

$$\sigma_c(\varepsilon_c) = \sigma_m(\varepsilon_c)V_m + \eta_l\eta_\theta\sigma_f(\varepsilon_c)V_f \tag{7}$$

In Eq. (7), η_l which represents the length efficiency factor in the pre-cracking case for frictional stress transfer mechanism, is defined as the following.

$$\eta_l = \overline{\sigma}_f(\varepsilon_c) / \sigma_f(\varepsilon_c) \tag{8}$$

where $\sigma_f(\varepsilon_c)$ represents the tensile stress at a strain of ε_c in the fiber. Substituting Eq. (6) into Eq. (8), η_l can be calculated as:

$$\eta_l = \frac{1-\tanh\beta_1 l/2}{\beta_1 l/2} \tag{9}$$

The fiber orientation coefficient, η_θ, depends upon the length of fiber, the effect of friction on the interface between the matrix and the fiber, etc. However, for simplicity, the geometrical arrangement of fiber is only considered; thus, the fiber orientation coefficient can be defined as given in Eq. (10) [29].

$$\eta_\theta = \int_{\theta_{\min}}^{\theta_{\max}} p(\theta)\cos^2\theta d\theta \tag{10}$$

where $p(\theta)$ is a probability density distribution for the fiber orientation and θ represents the angle between each fiber axis and the stress direction. It is found that η_θ has the value of 0.5 for a random 2-dimensional arrangement and 1/3 for a random 3-dimensional arrangement.

Eq. (10) indicates $\eta_\theta = 1$, when all the fibers are aligned parallel to the tensile stress direction; $\eta_\theta = 0$ conversely implies that all the fibers are aligned perpendicular to the tensile stress direction. This is derived from the assumption that there is no improvement of strength when the fibers are aligned perpendicular to the tensile stress direction, whereas the strength of composites is maximized when the fibers are aligned parallel to the tensile stress direction.

Fig. 2 compares the pre-cracking tensile behaviors of UHPFRCC, calculated using Eq. (7), for different fiber orientation coefficient values with 2 vol.% of fibers. The tensile strain at the first cracking (ε_{cr}) was assumed to be 236$\mu\varepsilon$, which was obtained by several previous experiments. As shown in Fig. 2, in the pre-cracking tensile behavior, although the elastic modulus as well as the first cracking strength improves as the fiber orientation coefficient increases, the improvement is limited within about 10%.

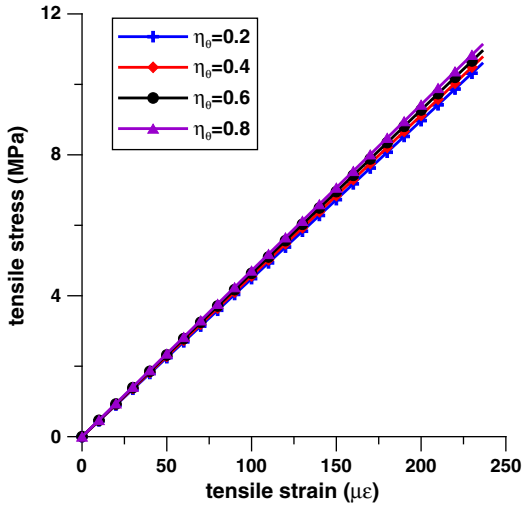

Fig. 2. Tensile behavior according to fiber orientation coefficient before cracking occurs in UHPFRCC.

2.2. Post-cracking tensile behavior

2.2.1. Modeling of tensile behavior by single fiber

In FRC composites, the major role played by the fibers is in the post-cracking zone. Once any cracking occurs, the cracked matrix no longer resists the tensile load and only fibers resist the load. Therefore, the characteristics of tensile behavior of the composites are determined by the pullout behavior of the fibers.

The pullout behavior of steel fiber, which is defined as the pullout load versus the end slip displacement, is divided into three regions: a perfectly bonded region, a partial debonding region, and a fully debonded region.

Lee et al. [30] proposed an analytical model to predict the pullout behavior of inclined steel fiber in an ultra high strength cementitious matrix. Both the matrix and steel fiber used in their study have exactly the same properties as those in this study. Their model was applied for the pullout behavior in this study. In their proposed model the bridging load (P) — the corresponding slip displacement (Δ) relation by a single fiber with an inclined angle (θ) can be expressed by Eq. (11) to Eq. (16):

– Perfectly bonded region

$$(P/\Delta)(\theta) = \frac{1}{1+\gamma(2\theta/\pi)^n}\frac{\lambda A_m E_m}{Q-2}\frac{1+e^{-\lambda l_e}}{1-e^{-\lambda l_e}} \tag{11}$$

– Partial debonding region

$$P(\theta) = \pi d_f \tau_{f(app)}(\theta)u + \frac{\pi d_f \tau_{\max(app)}(\theta)}{\lambda}\frac{1-e^{-2\lambda(l_e-u)}}{(2/Q)e^{-\lambda(l_e-u)} + (1-1/Q)\{1+e^{-2\lambda(l_e-u)}\}} \tag{12}$$

$$\Delta(\theta) = \frac{1+\gamma(2\theta/\pi)^n}{A_m E_m}\left\{\begin{array}{l} P(\theta)(Q-1)u - \frac{\pi d_f \tau_{f(app)}(\theta)u^2}{2}(Q-2) \\ + \left(P(\theta)-\pi d_f \tau_{f(app)}(\theta)u\right)\left(\frac{1-e^{-\lambda(l_e-u)}}{1+e^{-\lambda(l_e-u)}}\right)\frac{Q-2}{\lambda} - \pi d_f \tau_{f(app)}(\theta)u l_e \end{array}\right\} \tag{13}$$

– Fully debonded and frictional slip behavior region

$$x = \left(l_e^2 - \Delta l_e\right) / \left(l_e - \Delta_0\right) \tag{14}$$

$$P(\theta) = \pi d_f \tau_{fd}(\Delta)x \tag{15}$$

$$\tau_{fd}(\Delta) = \tau_{f(app)}(\theta)\exp\{-\eta(\Delta-\Delta_0)^\alpha\}\frac{1-\exp\left\{-4v_f\mu x / \left[E_f d_f\left(\frac{1+v_m}{E_m} + \frac{1-v_f}{E_f}\right)\right]\right\}}{1-\exp\left\{-4v_f\mu l_e / \left[E_f d_f\left(\frac{1+v_m}{E_m} + \frac{1-v_f}{E_f}\right)\right]\right\}} \tag{16}$$

where l_e means the embedded length of the fiber; A, E and v represent sectional area, elastic modulus and Poisson's ratio with subscript f for fiber and m for matrix; Δ_0 is the slip of the fiber at the end of full debonding; u is the debonding length; μ is the friction coefficient of the fiber–matrix interface; Q is easily calculated from the geometric information and physical properties of fiber and matrix; α, γ, η, λ and n can be determined through experiments of pullout behavior. $\tau_{\max(app)}$ and $\tau_{f(app)}$ were introduced to consider the effect of inclined fiber on the initial bond strength as well as frictional bond strength. Considering the snubbing effect and matrix spalling effect on the bond strength, Lee et al. [30] proposed the following equation as a function of θ.

$$\tau_{app}(\theta) = e^{f\phi}(\cos\theta)^{\kappa}\tau(\theta = 0) \quad (17)$$

A comparison with their experimental results revealed that $f = 1.6$ and $k = 1.8$ can be applied to both $\tau_{\max(app)}$ and $\tau_{f(app)}$ for UHPFRCC.

The fiber bridging stress (σ_b) versus crack opening displacement (δ) relation by a single fiber can be obtained from the pullout behavior. For the ascending branch, that is, before the fiber is fully debonded, a perfectly bonded region and a partial debonding region are included, and the crack opening displacement can be simply assumed as being two times the slip deformation in the pullout behavior, because slip occurs at both sides of the crack plane. For the descending branch where frictional slip behavior occurs after perfect debonding, the crack opening displacement is equal to the slip deformation in pullout behavior because slip occurs only at shorter fibers of the crack plane.

2.2.2. Modeling of tensile behavior by multiple fibers

When the pullout resistant force of a single fiber at the cracked plane is given as a function of the inclined angle of the fiber (θ), the embedded length of the fiber (l_e) and the crack opening displacement (δ), which is denoted as $P(\theta, l_e, \delta)$, the bridging stress of the composites may be obtained from Eq. (18) [15].

$$\sigma_b(\delta) = \frac{4V_f}{\pi d_f^2}\int_0^{\frac{\pi}{2}}\int_0^{\frac{l}{2}} P(\theta, l_e, \delta)p(l_e)p(\theta)\cos\theta dl_e d\theta \quad (18)$$

where $p(\theta)$ and $p(l_e)$ are probability density functions for θ and l_e respectively. For three-dimensional random distribution of fibers, $p(\theta)$ is $\sin\theta$ (see Fig. 3) and $p(l_e)$ is simply given by $2/l$.

In Eq. (18), $P(\theta, l_e, \delta)$ represents the bridging force acting on the fiber in a fiber-reinforced composite. The bridging force obtained from the pullout test, where the fiber is embedded in a plain matrix (without fiber) rather than in a composite, shows some difference compared with the actual bridging force in composites. Markovic [31] investigated the influence of fiber volume fraction in the pullout medium on the pullout behavior of the fiber. He used a mix design similar to the mix condition ($w/b = 0.2$) adopted in this study and the same properties of steel fibers and compared the fiber pullout behaviors in a plain matrix and a fiber-reinforced composite with 2 vol.% of fibers. He demonstrated that the presence of 2 vol.% of fibers in the plain matrix improved the maximum pullout force by about 25%. Based on the findings of his study, the pullout force in the composites $P(\theta, l_e, \delta)$ can be calculated from the pullout force obtained from the pullout test:

$$P(\theta, l_e, \delta) = \alpha_f P_{pullout}(\theta, l_e, \delta) \quad (19)$$

In the above equation, α_f is a coefficient that represents the relation between the pullout behavior in an actual composite and in a pullout test. $\alpha_f = 1.25$ was applied for UHPFRCC.

Fig. 4 shows the relation between fiber bridging stress and crack width, which is calculated by Eqs. (18) and (19) for two- and three-dimensional random distributions of fibers, respectively. It can be seen that the assumption of a two-dimensional random distribution leads to better performance than in the case of a three-dimensional random distribution.

Post-cracking behavior of a composite can be defined as the combined behavior of the resistance by the fibers and the matrix. Therefore, in addition to fiber bridging, the contribution of the matrix should be introduced in order to establish the post-cracking behavior. Typical tension softening behavior of concrete after cracking is depicted in Fig. 5; linear, bilinear, or exponential curves are generally accepted as reasonable approximation of the tension softening curves for concrete. In this study, the bilinear softening behavior proposed in CEB-FIP Model Code 1990 [32] was first considered. Strictly speaking, the matrix of UHPFRCC is not concrete but mortar without coarse aggregate. Therefore it is reasonable to adopt a tension softening curve of mortar rather than that of concrete. However, since we couldn't find any tension softening curve applicable to mortar in the literature review, there was no other choice but to apply that of

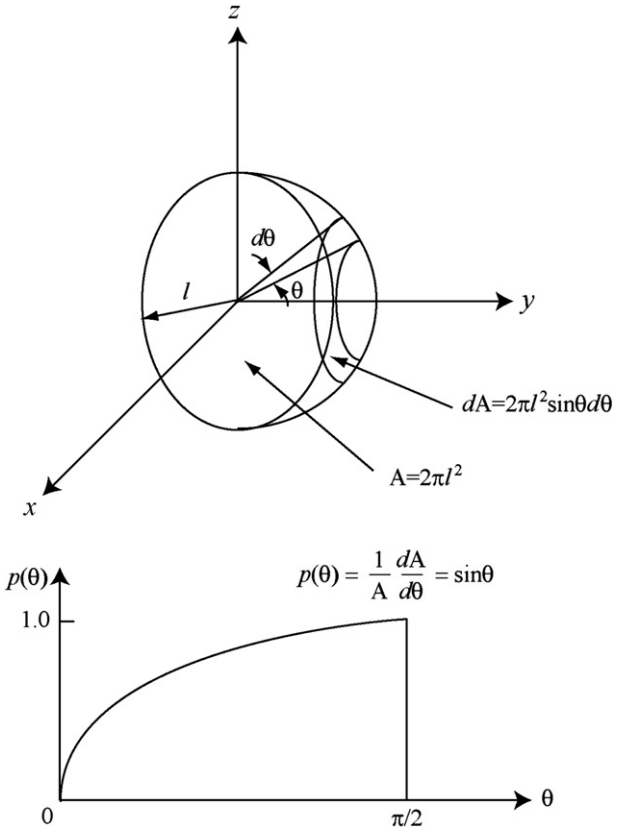

Fig. 3. Probability density distribution in 3-D randomly oriented fiber distribution [15].

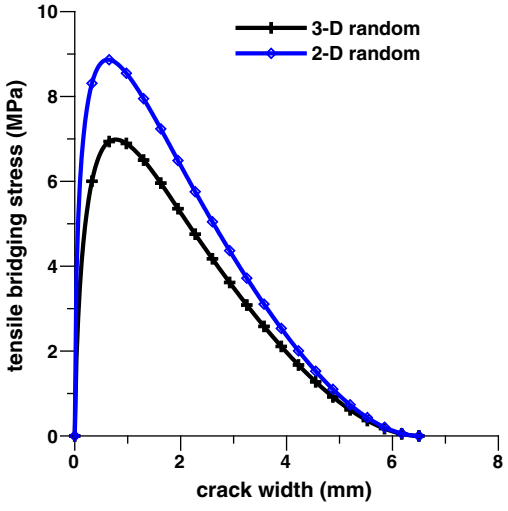

Fig. 4. Bridging behavior by fibers calculated with Eqs. (18) and (19) for 3-D and 2-D random fiber distributions.

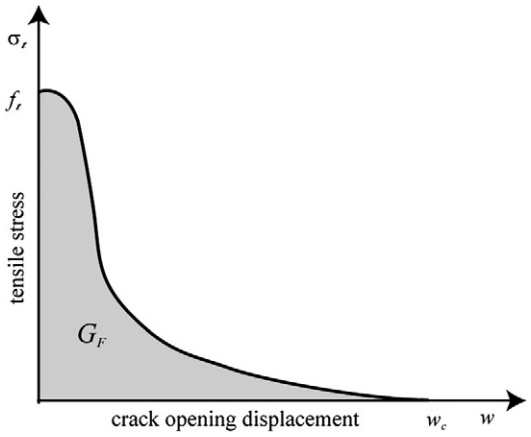

Fig. 5. Typical tension softening curve of concrete.

concrete with reduced aggregate size. The bilinear stress-crack opening relation is given by the following equations.

$$\sigma_{ct} = f_t\left(1-0.85\frac{w}{w_1}\right) \quad \text{for } 0.15f_t \le \sigma_{ct} \le f_t \tag{20}$$

$$\sigma_{ct} = \frac{0.15f_t}{w_c - w_1}(w_c - w) \quad \text{for } 0 \le \sigma_{ct} \le 0.15f_t \tag{21}$$

$$w_1 = 2G_F / f_t - 0.15w_c \tag{22}$$

$$w_c = a_F G_F / f_t \tag{23}$$

where f_t is the tensile strength, w is the cracking opening (mm), and σ_{ct} is the tensile stress at a given crack opening. w_1 is the cracking opening (mm) at $\sigma_{ct} = 0.15f_t$, w_c is the cracking opening (mm) at $\sigma_{ct} = 0$, G_F is the fracture energy (Nm/m^2), and a_F is the coefficient as a function of the maximum aggregate size. The fracture energy of the pure UHPFRCC matrix without fibers was assumed as 30 Nm/m^2 [33]. The pure matrix is known to be in the range of 12 to 50 Nm/m^2 for the fracture energy.

3. Experiments

The mix design of UHPFRCC differs significantly from that of normal concrete. UHPFRCC mix proportion applied in this study is given in Table 1. The water-binder ratio is determined as $w/b = 0.2$. Sand with grain size below 0.5 mm is used as fine aggregate, and coarse aggregates are excluded. Superplasticizer has been introduced to secure the required workability for a low water to binder ratio composition. In addition, the filler used to enhance the density of UHPFRCC has mean grain size of about 4 μm. 2 vol.% of straight steel fibers with 13 mm length and 0.2 mm diameter were incorporated. The property in a fresh state was evaluated by a flow test (ASTM C1437) and the flowability was measured to be about 230 mm.

Experiments on the effect of fiber orientation on the tensile behavior of the composites were carried out, and those were compared with the analytically obtained results. The comparison provides verification of the analytical approach for the tensile behavior of the composites and also highlights any parts of the analytical model that require modification.

Table 1
Mix design of UHPFRCC.

Relative weight ratios to cement						Steel fiber (V_f [a], %)
Cement	Water	Silica fume	Fine aggregates	Filler	Superplasticizer	
1.00	0.25	0.25	1.10	0.30	0.018	2

[a] Fiber volume expressed as a volumetric ratio to the whole volume.

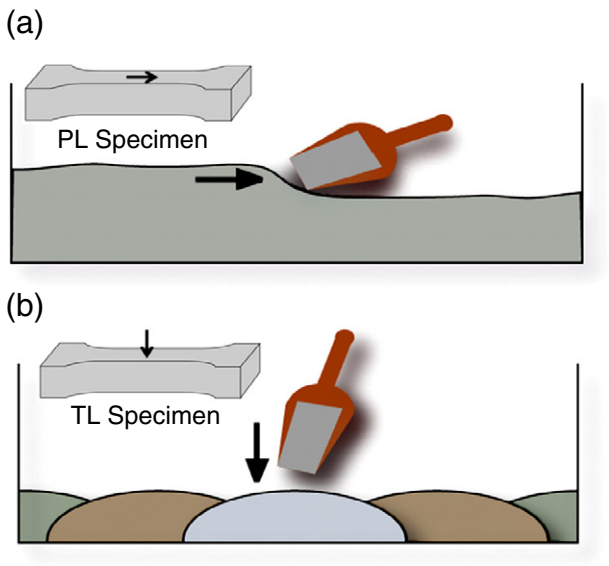

Fig. 6. Specimen preparation by (a) placing concrete parallel to the tensile direction of the specimen; and (b) placing concrete transversely to the tensile direction of the specimen.

As noted previously, pre-cracking behavior shows no significant difference and, moreover, it is difficult to distinguish small variation in the tensile behavior depending on the fiber orientation from the experimental results. Therefore, the main focus of the experimental verification is on the post-cracking behavior.

3.1. Test method

In order to investigate the effect of the fiber orientation distribution on the tensile behavior, two types of fiber orientation distribution were induced by adopting different placing directions (see Fig. 6).

Two cases were considered for the placing directions: placement parallel to the tensile direction of the specimen and placing concrete transversely to the tensile direction. Fig. 6 illustrates each of the placing directions adopted for the manufacture of the specimens.

Direct tensile tests were conducted on notched specimens. Specimens for the direct tensile test were fabricated in the so-called dog-bone shape. Prior to the test, 10 mm notches were made on both sides at the center of the specimens as shown in Fig. 7(a). The direct tensile test was carried out in the way as depicted in Fig. 7(b).

The direct tensile test set-up was designed with a so-called pin-fixed ends in order to avoid secondary flexural stress as well as to assure the centricity of loading [34]. In Japan, this boundary condition was adopted as a standard in the tensile test for strain-hardening cementitious composites [35]. The direct tensile test was implemented using a 250 kN capacity universal testing machine with a loading rate of 0.2 mm/min. As each specimen was being tested, its crack mouth opening displacement (CMOD) in the notch was measured by clip gages placed on two opposite sides of the specimen.

3.2. Experimental results

Table 2 gives the measured stresses and CMODs at the moment of first cracking as well as maximum stresses for two cases of placement directions, respectively. The first cracking strength is defined as the stress at the point when the initial behavior loses the linearity. In Table 2, the label 'PL' denotes the case of placement parallel to the

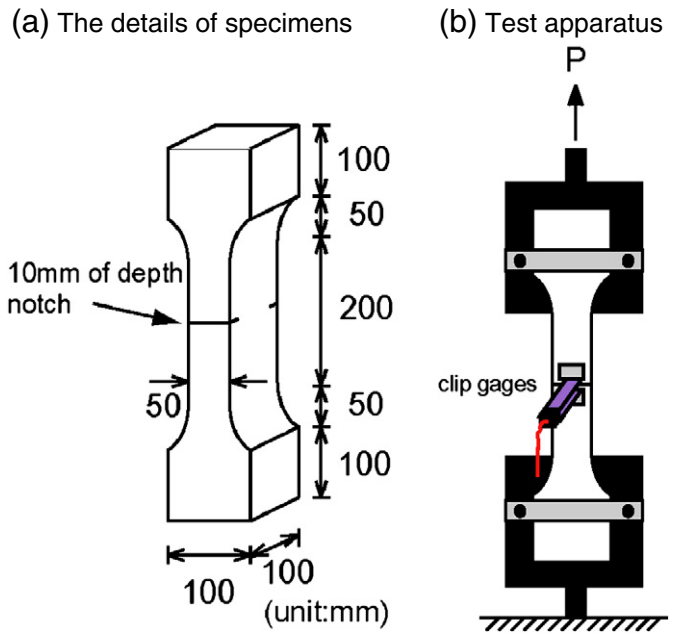

Fig. 7. Direct tensile test specimen and apparatus.

tensile direction of the specimen and 'TL' denotes the case of placing concrete transversely to the tensile direction. Fig. 8 zooms into the initial tensile behaviors including the first cracking for both the PL and TL specimens. The average of the first cracking stress is 10.93 MPa for the PL specimens and 9.96 MPa for the TL specimens, respectively. Fig. 9 exhibits the overall tensile behaviors for the TL and PL specimens. The average maximum tensile stress is 16.05 MPa for the PL specimens and 11.80 MPa for the TL specimens. The experimental results verify that there is a remarkable difference in the tensile behavior according to the placing direction; PL specimens show better performance than TL, and the difference in tensile stress between the two cases is much greater at the maximum stress than at the first cracking. For the first cracking stress, the PL specimens exhibit approximately 10% higher stresses than the TL specimens. Meanwhile, for the maximum stress, the former is greater than the latter by 40%.

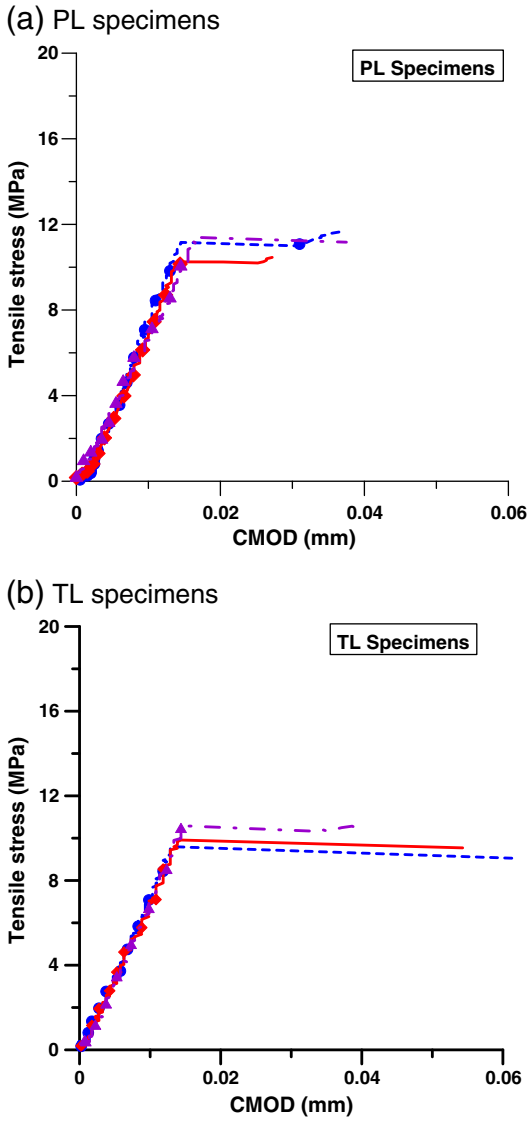

Fig. 8. Initial tensile behaviors including the first cracking.

4. Analysis and discussion

4.1. Evaluation of fiber orientation distribution

In order to estimate the tensile behavior of UHPFRCC depending on fiber orientation distribution, the distribution characteristics of fibers in a composite should be quantitatively evaluated in advance. For this purpose, an image processing technique proposed by Lee [36] was adopted. The images were obtained by using high-resolution camera.

The distribution characteristics of fiber can be quantitatively evaluated by calculating coefficients based on the coordinates of fibers and the shape of the fibers in the cutting plane. To detect the fiber in the fiber images, the RGB image (Fig. 10(a)) is converted to a grayscale image (Fig. 10(b)). The grayscale image is then converted to a binary image (Fig. 10(c)) based on a set threshold object detection method. In this process, the fibers can be distinguished from the surrounding and other objects on the criteria of brightness and area. The distribution characteristics of the fiber in the detected fiber images are represented quantitatively by several coefficients.

First, the degree of fiber dispersion is quantitatively evaluated based on calculation of the coefficient α_f, referred to as the fiber dispersion coefficient, as expressed by Eq. (24) [37].

$$\alpha_f = \exp\left[-\sqrt{\frac{\sum(x_i-1)^2}{n_f}}\right] \tag{24}$$

where n_f is the total number of fibers on the image and x_i denotes the number of fibers in the i-th unit, which is one of equivalent

Table 2
Direct tensile test results.

Specimen no.	At first cracking		At maximum	
	Stress (MPa)	CMOD (mm)	Stress (MPa)	CMOD (mm)
PL1	11.16	0.014	16.04	0.398
PL2	10.25	0.016	16.03	0.144
PL3	11.39	0.017	16.08	0.469
Mean (St. dev.)	10.93 (0.60)	0.016 (0.001)	16.05 (0.03)	0.337 (0.171)
TL1	10.44	0.015	12.67	0.204
TL2	9.55	0.014	10.67	0.184
TL3	9.88	0.014	12.06	0.240
Mean (St. dev.)	9.96 (0.45)	0.014 (0.001)	11.80 (1.03)	0.209 (0.028)

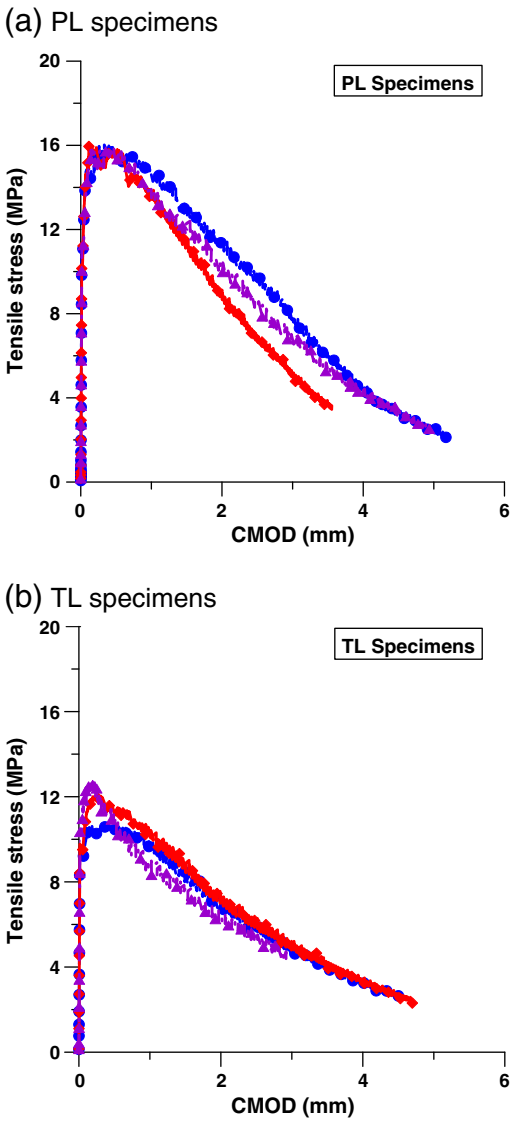

Fig. 9. Overall tensile behaviors.

squares divided from the total area. The value for α_f tends to 1 for a homogeneous dispersion of fibers, or 0 for a severely biased dispersion.

The second coefficient is F_n, which is the number of fibers in a unit area, and is expressed by Eq. (25).

$$F_n = \frac{n_f}{A} \tag{25}$$

where A is the area of the image.

The third coefficient is the packing density F_c, which is defined as the division of an object's area by that of the object's circumscribed circle, as expressed by Eq. (26).

$$F_c = \frac{A_{ob}}{A_{cc}} \tag{26}$$

where A_{ob} represents an object's area and A_{cc} means the area of the object's circumscribed circle. The value for F_c tends toward 0 for an extremely elongated object like slender long cylinder or 1 for a circular object. F_c is useful for calculating the inclined angle of the fiber to the cutting plane (Fig. 11), as expressed by Eq. (27).

$$F_c = \frac{\pi d_f l/4}{\pi l/4} = \frac{d_f}{l} = \frac{d_f}{d/\cos\theta} = \cos\theta \tag{27}$$

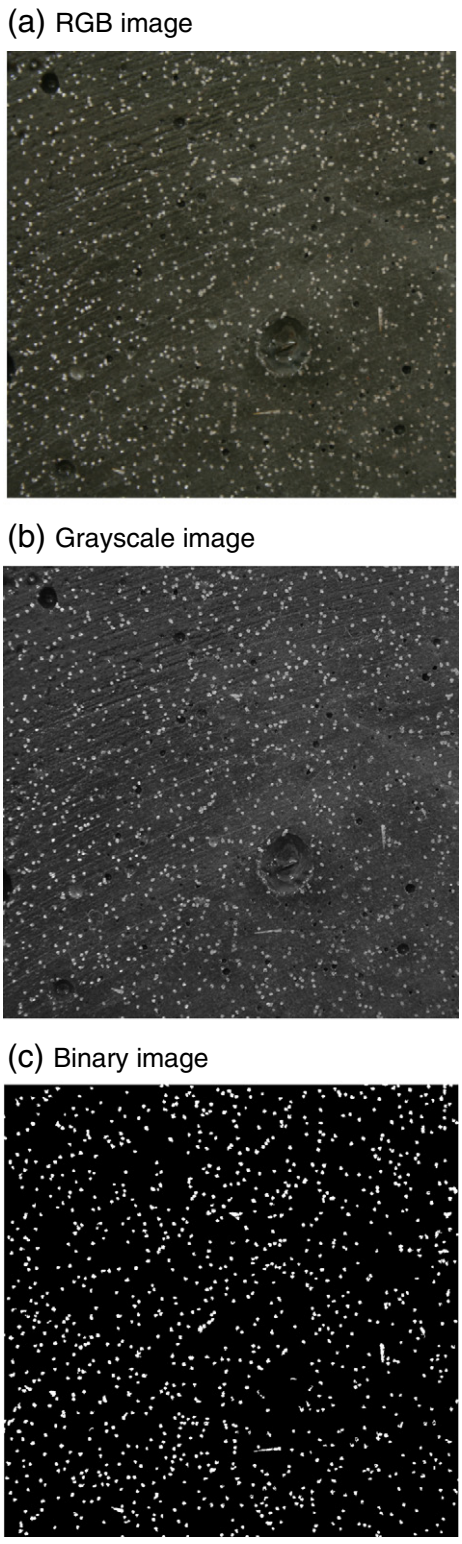

Fig. 10. Image transformation for detecting fiber distribution (in case of PL2): (a) RGB image, (b) grayscale image and (c) binary image.

where θ, d_f, and l are the inclined angle of the fiber, the diameter of the fiber, and the major axis length of the fiber image, respectively.

The last is the fiber orientation coefficient (η_θ), which is calculated by Eq. (10) considering F_c of each fiber as well as probability density distribution of the fiber orientation.

In order to evaluate the orientation of the fibers according to the placement directions of UHPFRCC, the specimens were cut at the cross

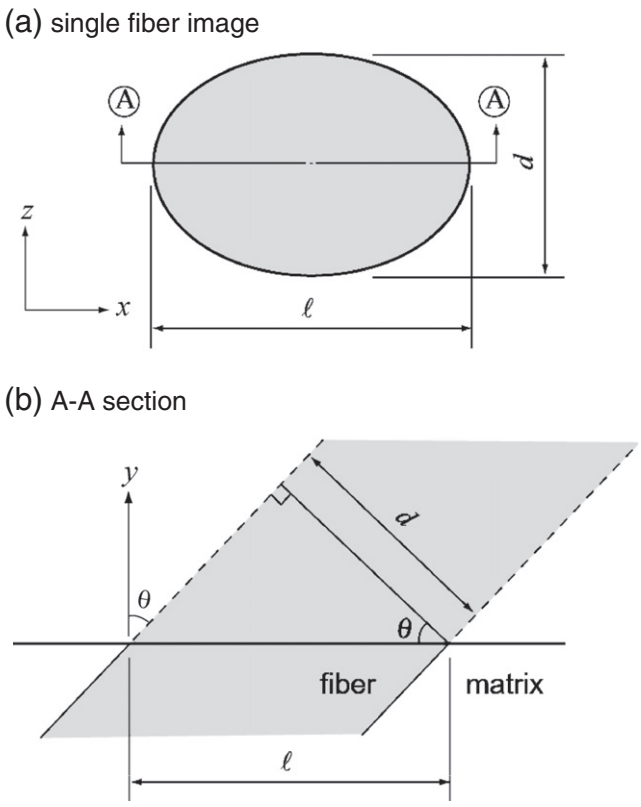

Fig. 11. Basic dimensions of inclined fiber; (a) plan view on the cutting plane; and (b) side view at the section of A–A [36].

section, i.e., normal to the tensile direction, as close as possible to the cracked plane after conducting tensile tests in order to obtain images of the cross section. High resolution photographs were taken at the cross sections to evaluate the orientation of the fibers. Digital images were analyzed using the image processing technique.

The obtained images of the fiber distribution are presented in Fig. 12, where it can be seen that in the case of concrete placed parallel to the tensile direction of the specimen (PL specimens), the fibers are more uniformly dispersed compared to TL specimens. Furthermore, most of the fibers in the PL specimens are aligned more parallel to the normal direction of the cut plane, relative to the TL specimens.

Fig. 13 presents the probability density distribution of fiber orientation for each specimen. It can be easily found that the fiber orientation distribution of the PL specimens is a left-skewed distribution whereas the TL specimens show a right-skewed distribution, which means that the fibers in the PL specimens have a tendency to be aligned so that they are more perpendicular to the cut plane (i.e. parallel to the tensile direction) whereas the fibers in the TL specimens are more parallel to the cut plane (i.e. perpendicular to the tensile direction). For the purpose of comparison, the probability density distributions of 2-D random distribution and 3-D random distribution are presented together. Fig. 14 presents a comparison of the probability density distribution of fiber orientation for the aforementioned 4 cases; the probability distributions of PL1, TL3, 2-D random, and 3-D random. Actual fiber orientation distributions (PL1 and TL3) in the specimens are quite different from idealized orientation distributions (2-D and 3-D random). This discrepancy seems mainly due to the flow pattern of fresh composites and the fiber movement in translation and rotation during placing, but the mechanism and quantification has not been clearly made yet.

Table 3 shows the fiber distribution characteristics. F_n (the number of fibers per unit area) of the PL specimens is equivalent to 0.351 and roughly 50% higher than that of the TL specimens (0.221), which is closely related to the fiber orientation distribution. In terms of the fiber dispersion coefficient, α_f of the PL specimens (0.407) is about 10% higher than that of the TL specimens (0.375), but there is no significant difference in the A_f/A_c ratio, where A_c represents the area of an image and A_f denotes the total area of fibers in the image. Concerning the fiber orientation coefficient (η_θ), PL specimens have higher values than TL specimens. η_θ is related to pre-cracking behavior and first cracking strength of a composite as mentioned earlier. Compared with the values for 2-D and 3-D random fiber distributions, the obtained coefficients are considerably different from those of the idealized distributions. PL specimens present higher coefficient than 2-D as well as 3-D, while TL specimens have a coefficient between the values for 2-D and 3-D. The results also indicate that assumption of idealized distribution is far apart from reality in placement and the distribution is considerably affected by placing condition.

4.2. Estimation of fiber bridging behavior

From the probability density distributions of fiber orientation, fiber bridging behaviors can be obtained by means of Eqs. (18) and (19). Fig. 15 presents the obtained fiber bridging behaviors for the PL and TL specimens. It can be seen that the fiber orientation distribution significantly affects on the fiber bridging behavior. Comparison also reveals that there is no noticeable variation among the bridging behaviors in each case. Considering the variation of the degree of fiber dispersion (α_f in Table 3) in each case as well as its difference on average between PL and TL specimens, it can be estimated that the difference in fiber dispersion between two cases is not considerable enough to cause noticeable variation in the bridging behavior. Therefore the obtained fiber distributions demonstrate that it is reasonable to estimate only the effect of fiber orientation distribution on the tensile behavior of the composites without any other variables.

PL1 and TL3 present median behaviors for each case. Thus, hereafter, those are adopted as representatives of the PL and TL specimens for analyzing the effect of fiber orientation distribution or for comparison with experimental results.

4.3. Comparison and analysis for the tensile behavior of the composites

For pre-cracking behavior, test results revealed that the first cracking stresses in the PL specimens were higher than in the TL specimens. This finding is coincident with the analytical results that a higher fiber orientation coefficient increases the first cracking stress, as described previously. When the first cracking is calculated by Eq. (7), the average fiber orientation coefficient of PL specimens (0.645) produces the first cracking strength of 10.98 MPa and that of TL specimens (0.431) leads to the strength of 10.79 MPa. Compared with experimental results, the calculated first cracking strength shows much smaller difference according to the value of fiber orientation coefficient. However, it should be noted that it is very difficult to quantitatively evaluate the small difference in the first cracking strength due to fiber orientation distribution through the experiment since there is always a little variation in experimental results due to many reasons enough to influence on the difference significantly. In addition, the difference according to the fiber orientation distribution is not as great as in the post-cracking behavior. Therefore, the comparison and analysis is mainly focused on the post-cracking behavior.

As noted earlier, post-cracking behavior of a composite can be described as the combined behavior of the resistance by the fibers and the matrix, and for the tension softening curves for the matrix, the bilinear softening behavior proposed in CEB-FIP Model Code 1990 [32] was adopted first in the analysis.

Fig. 16 compares the analytically obtained post-cracking behaviors with experimental results for the PL and TL specimens. The softening behaviors show a similar tendency between the analytical and

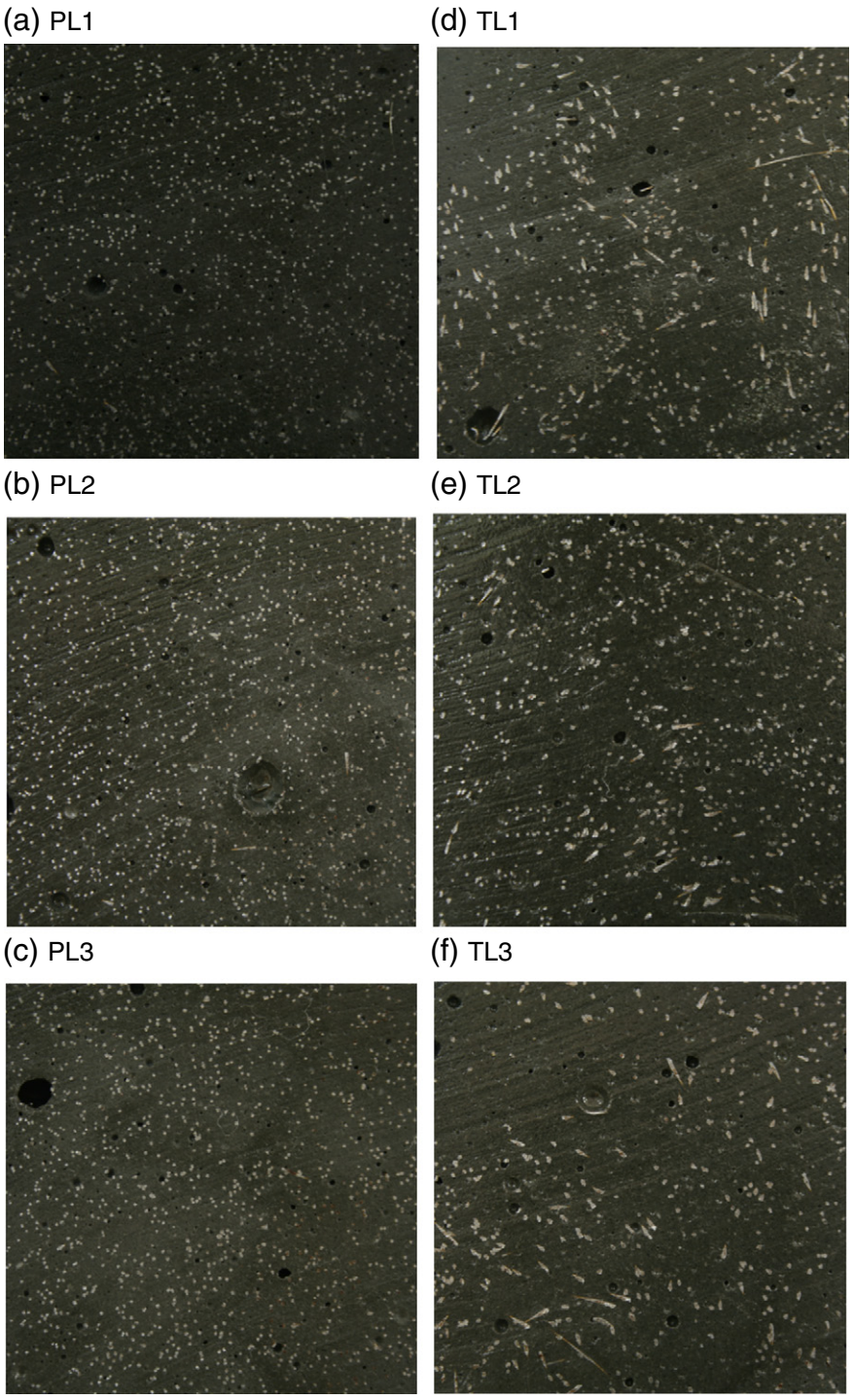

Fig. 12. Digital images of fiber distribution for PL and TL specimens.

experimental results for the two cases, but the ascending behavior and the peak stress show noticeable difference between the analytical and experimental results. It can be said that the analytical solutions underestimate the post-cracking behavior of the composites.

The difference can be attributed to two major reasons. The first is the bond condition at the interface between the matrix and the fiber. The bridging behavior is obtained based on the pullout test results. However, the bond condition in the pullout test is not precisely equal to that in an actual composite mixed in a conventional manner. The second is that the softening behavior of the matrix appears to be different when it is mixed with fibers. In Fig. 16, it is found that the analytically obtained tensile behavior of the composites exhibits a sudden stress drop and recovery as soon as cracking occurs, but this did not occur in the experimental results. Considering this difference in the tensile behavior, the tension softening of the matrix may occur very slowly, rather than suddenly in a narrow crack opening range such as in the CEB-FIP Model Code 1990 [32]. Generally, even if a tiny notch was given in the center of the prism, the presence of fibers in the matrix might cause multiple cracking inside of the ligament. The presence of multiple cracking during the crack propagation process could be observed in the

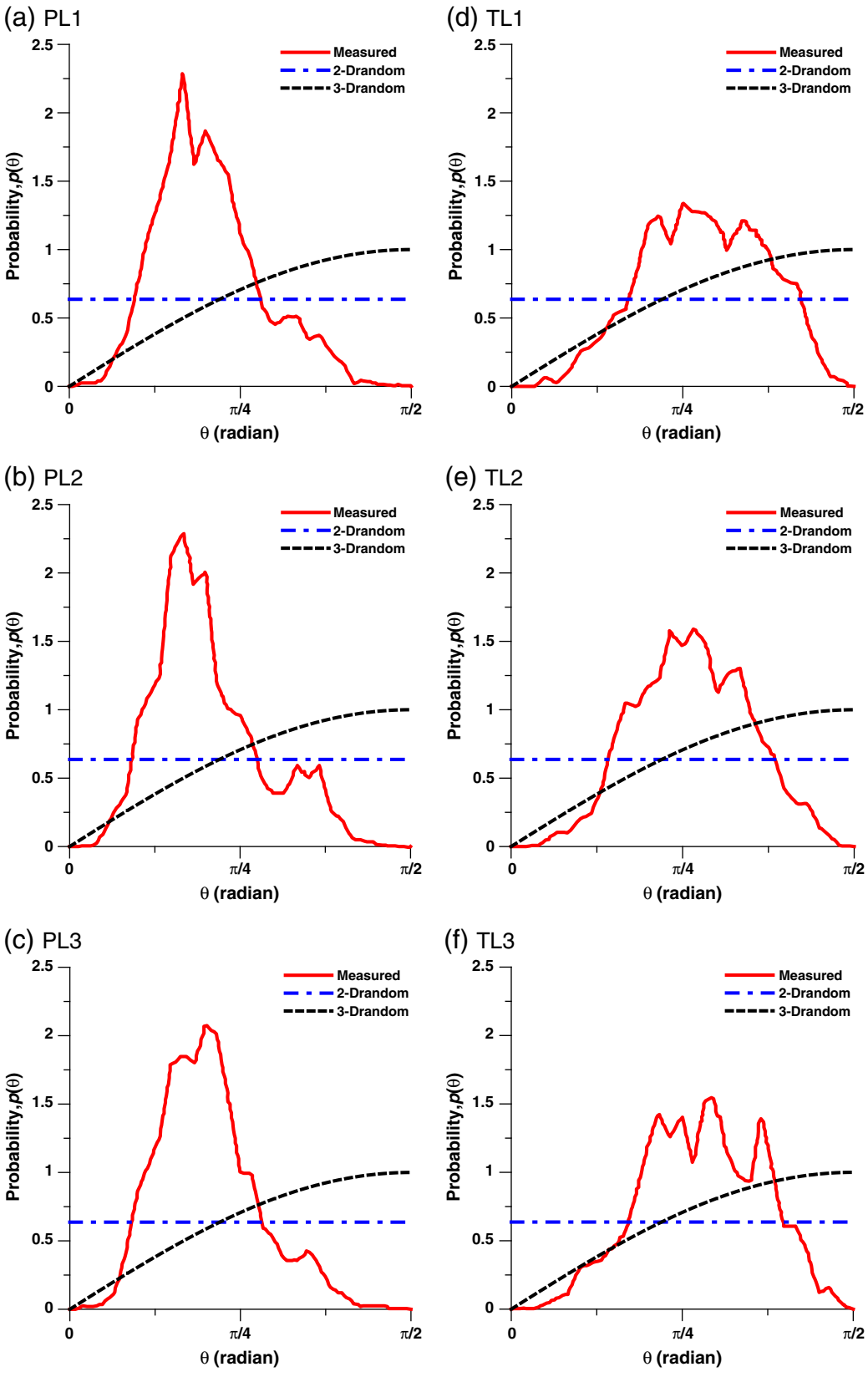

Fig. 13. Probability density distributions for PL and TL specimens.

experiment on the notched specimens. Therefore the softening behavior of matrix could seem to be much more ductile than its own natural softening behavior. Strictly speaking, it is not original tension softening curve of matrix in UHPFRCC. We therefore defined the phenomenological softening behavior of matrix in the composites as 'apparent tension softening curve of matrix' considering the effect of added fiber. Thus it can be explained that the matrix in the composites may present much better resistance and increased energy absorbing capacity in post-cracking

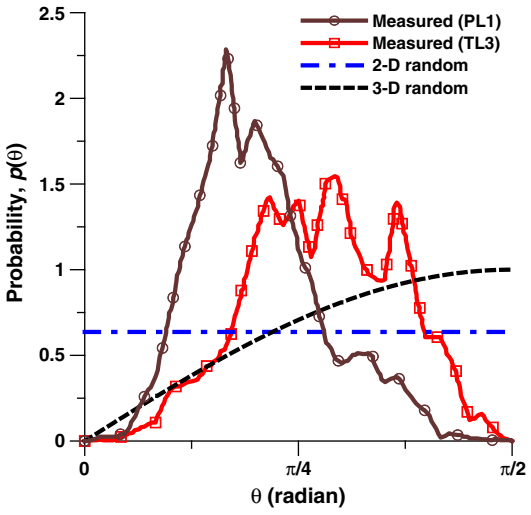

Fig. 14. Comparison of the probability density distribution of fiber orientation.

behavior. This apparent tension softening may be dependent on the characteristics of fiber (aspect, length, volume fraction, etc.) as well as matrix properties (strength, aggregate size, etc.).

The consideration of the first reason can be reflected in Eq. (28), and thus Eq. (19) is replaced by the following equation.

$$P(\theta, l_e, \delta) = \alpha_f \beta_f P_{pullout}(\theta, l_e, \delta) \tag{28}$$

where β_f represents a coefficient to consider the actual bond condition in the composites. Comparison with the experimental results shows that $\beta_f = 1.2$ can be applied to UHPFRCC.

In order to correct the error resulting from the second reason, we attempted to extract the apparent tension softening curve of the matrix in UHPFRCC from the direct tensile test results of UHPFRCC. The post-cracking curve obtained from the direct tensile test is the combined behavior of matrix softening and fiber bridging behavior. Consequently, the apparent matrix softening behavior can be assumed to be obtained by subtracting the fiber bridging curve from the post-cracking curve of the composites. The obtained apparent tension softening behavior of the matrix is given in Fig. 17. The test results of the PL and TL specimens were used, and as the fiber bridging behaviors, the analytic curves obtained from the fiber orientation distribution were applied. The results are plotted as a relation between the ratio of tensile stress to strength (σ_t/f_t) and CMOD.

As shown in Fig. 17, the apparent tension softening behaviors appear to be similar for all specimens regardless of the fiber bridging behaviors, and can be expressed by a bilinear softening curve for simplicity. The following equations can be applied for the apparent softening curve of the matrix in UHPFRCC.

$$\sigma_{ct} = f_t\left(1 - 0.7\frac{w}{w_c}\right) \quad \text{for } 0.3f_t \le \sigma_{ct} \le f_t \tag{29}$$

$$\sigma_{ct} = \frac{0.3f_t}{w_c - w_1}(w_c - w) \quad \text{for } 0 \le \sigma_{ct} \le 0.3f_t \tag{30}$$

$$w_1 = 0.2\,\text{mm}, \text{ and } w_c = 0.5\,\text{mm} \tag{31}$$

Table 3
Fiber distribution characteristics.

		α_f	F_n (number/mm^2)	A_f/A_c	η_θ
PL specimens	PL1	0.396	0.372	0.054	0.635
	PL2	0.411	0.307	0.066	0.658
	PL3	0.414	0.375	0.055	0.642
	Mean (st.dev.)	0.407 (0.010)	0.351 (0.038)	0.058 (0.007)	0.645 (0.011)
TL specimens	TL1	0.364	0.201	0.064	0.411
	TL2	0.392	0.228	0.056	0.459
	TL3	0.370	0.235	0.062	0.422
	Mean (st.dev.)	0.375 (0.015)	0.221 (0.018)	0.060 (0.004)	0.431 (0.025)

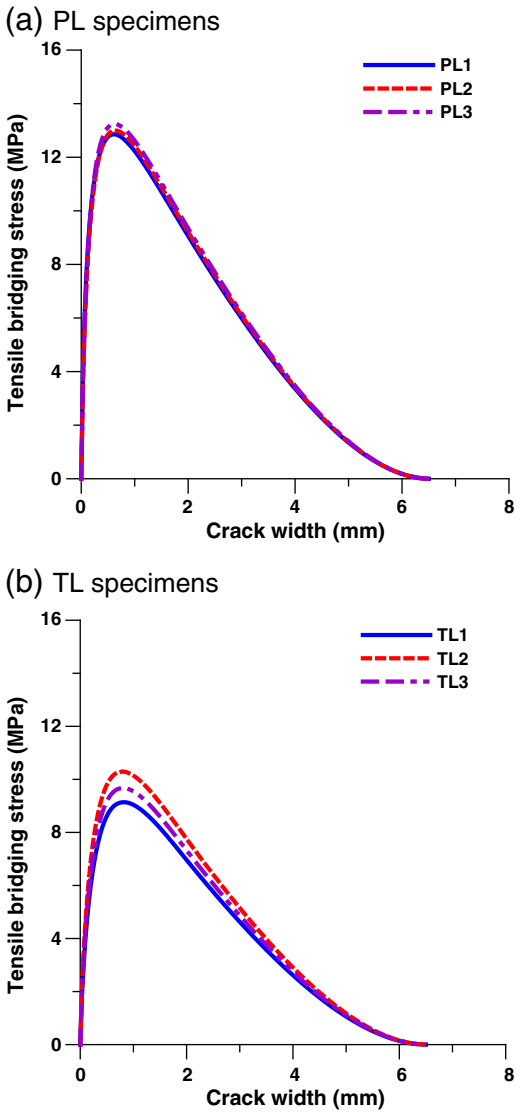

Fig. 15. Calculated fiber bridging behaviors of PL and TL specimens.

From the apparent tensile softening curve of the UHPFRCC matrix, an 'apparent specific fracture energy' which is defined as the area under the curve can also be determined. The calculated value is 1750 Nm/m^2 when the tensile strength is assumed as 10 MPa. Considering the first assumed G_F value for the pure UHPFRCC matrix was 30 Nm/m^2, the apparent specific fracture energy is much higher.

Fig. 18 compares the fiber bridging behaviors obtained from Eqs. (18) and (28) for four cases with each fiber orientation distribution. The PL specimen shows much better tensile performance than the others. The TL specimen is also better than the cases with 2-D and 3-D random fiber distributions, although its performance does not equal that of the PL specimen.

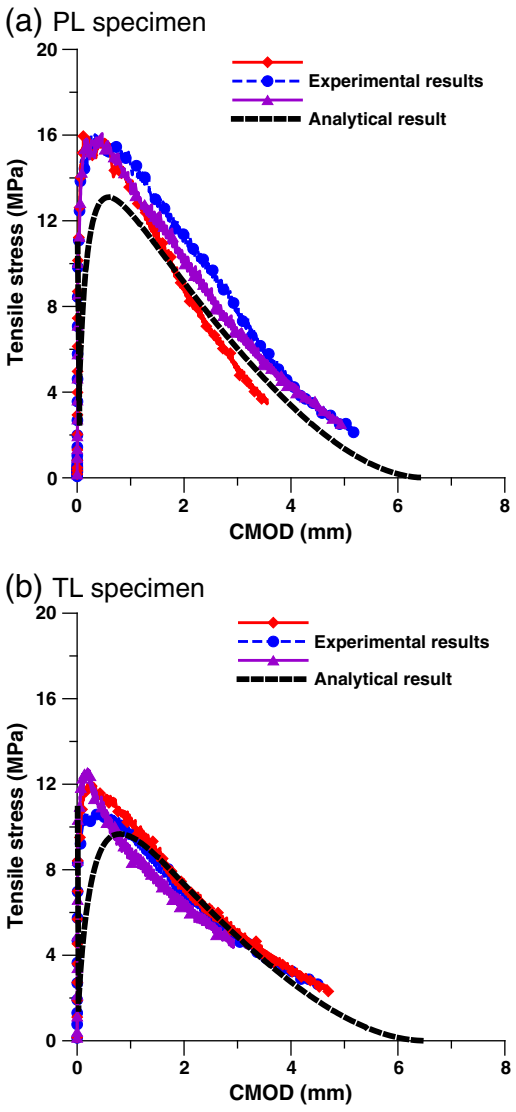

Fig. 16. Comparison between experimental and analytical results.

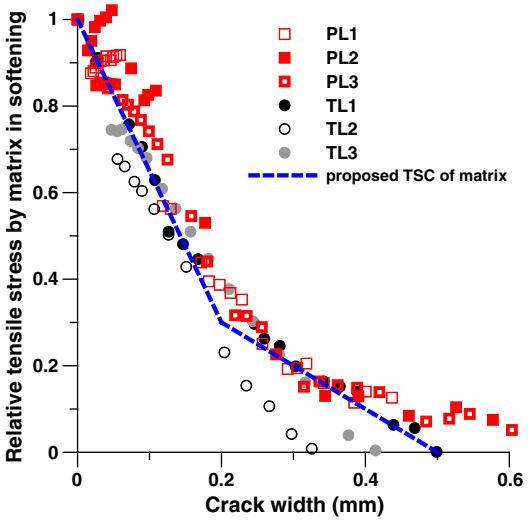

Fig. 17. Apparent tension softening behavior of matrix in UHPFRCC.

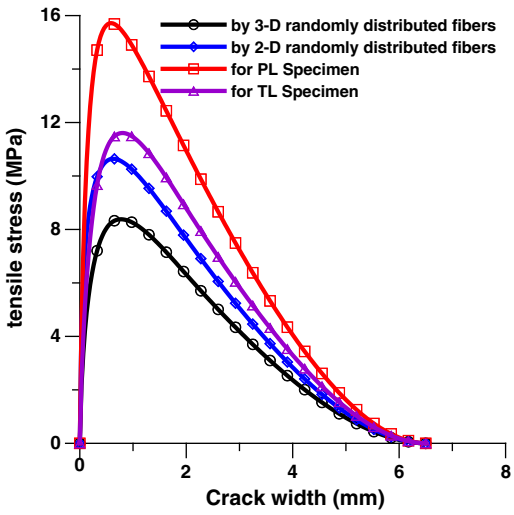

Fig. 18. Comparison of modified fiber bridging behaviors for different fiber orientation distributions.

The combined post-cracking tensile behavior is depicted in Fig. 19. Fig. 19(a) shows the initial behaviors up to a crack width of 0.2 mm, and Fig. 19(b) shows the overall tensile behaviors. As can be seen in Fig. 19, the post-cracking tensile behavior is strongly dependent on the fiber orientation distribution, and the comparison shows that the post-cracking tensile strength can be considerably different according to the fiber orientation distribution; the post-cracking tensile strength of the PL specimen is about 50% higher than that of 3-D randomly distributed fibers. In addition, no sudden drop of stress is found in the initial behavior, and thus it can be said that the adoption of the apparent matrix softening curve allows more precise expression of the post-cracking tensile behaviors.

When compared with the experimental results of the PL and TL specimens, the analytic approach appears to predict the post-cracking tensile behaviors closely, especially for PL specimens, as can be seen in Fig. 20. Concerning the TL specimens, the post-cracking tensile strength as well as the behavior up to about 0.6 mm CMOD is predicted well, after which, however, the softening behavior appears to be slightly over-estimated. Nevertheless, it can be said that the prediction of post-cracking tensile behavior from the actual fiber orientation distribution is in relatively satisfactory agreement with the experimental results.

5. Conclusions

In this paper, the effect of the fiber orientation distribution on the tensile behavior of UHPFRCC was investigated. The tensile behavior was explored separately in two stages, pre-cracking and post-cracking tensile behaviors.

(1) Pre-cracking tensile behavior is expressed using the mechanism of elastic shear transfer between the matrix and the fiber in the composites. The analysis revealed that improvement of the first cracking strength by the fiber orientation was limited to 10% for the entire range of the fiber orientation coefficient. Experimental results verified that a higher fiber orientation coefficient increases the first cracking stress slightly.

(2) In order to predict fiber bridging behavior, a probability density function for the fiber orientation distribution across the crack surface and a pullout model of steel fiber were considered. Four cases with different fiber orientation distributions were investigated: 2D and 3D random distributions, and fiber orientation distributions acquired from an image analysis for 'PL' (the case of placing parallel to the tensile direction of the specimen) and 'TL' (the case of placing transversely to the tensile direction

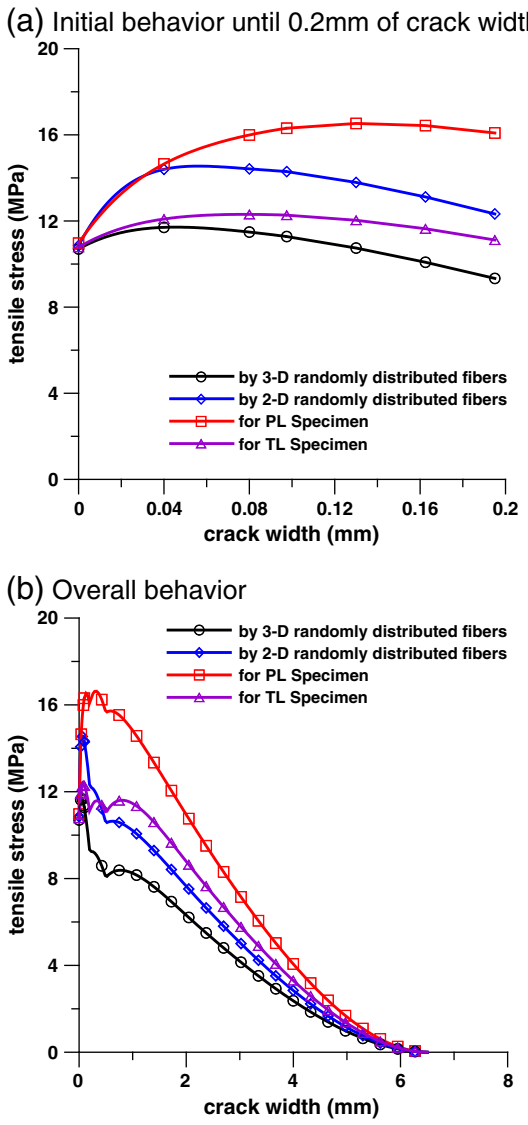

Fig. 19. Comparison of post-cracking tensile behaviors for 4 different cases.

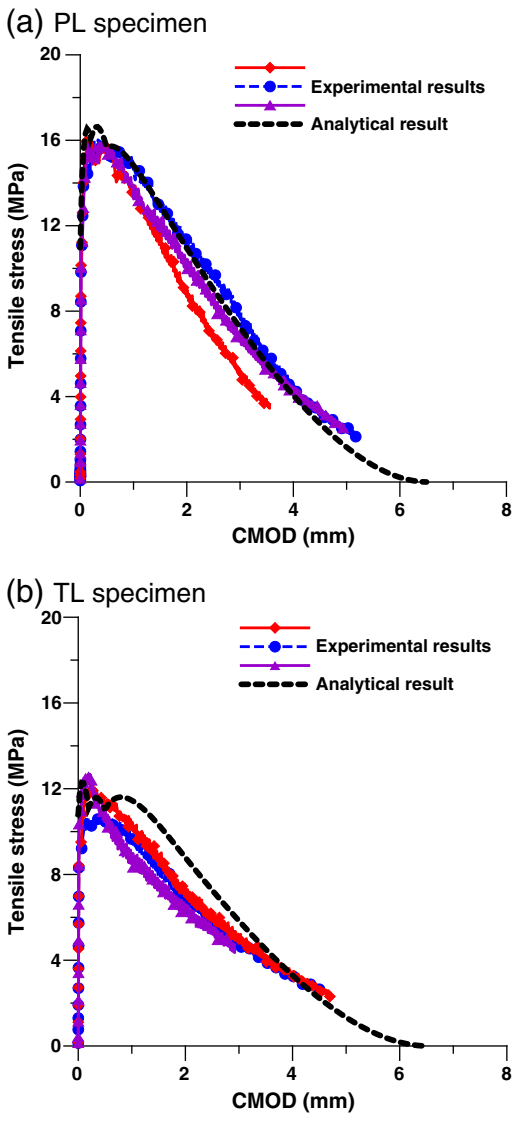

Fig. 20. Comparison between experimental and analytical results.

of the specimens) considered in the experimental program. The comparison revealed that fiber orientation distribution had a strong impact on the fiber bridging behavior.

(3) Post-cracking tensile behavior of the composites was defined as the combined behavior of the resistance by the fibers and the matrix. Tension softening behavior of the mortar in UHPFRCC was found to be different from the typical softening curve of concrete. In this research, the apparent matrix softening behavior in UHPFRCC was studied under the assumption that the resistant behavior by mortar could be thought equal to the actual post-cracking curve minus the fiber bridging curve, and a simplified bilinear softening curve that was applicable to the matrix in UHPFRCC was suggested.

(4) For the purpose of verification of the proposed analytical method, an experimental investigation was performed. Direct tensile test was carried out and the results were compared with the analytical results. The comparison demonstrated that the analytical approach estimated the effect of the fiber orientation distribution on the tensile behavior of UHPFRCC reasonably well and the predicted tensile behaviors showed satisfactory agreement with the experimental results.

Acknowledgments

This work was financially supported in part by Korea Institute of Energy Technology Evaluation and Planning (KETEP) via the project “Improvement of Constructability for Optimizing NPP Construction”, and in part by Korea Institute of Construction Technology (KICT) via the project “Improvement in Performance of Marine Concrete”. The authors would like to express their gratitude for the supports.

References

[1] S.P. Shah, V.B. Rangan, Fiber reinforced concrete properties, J. Am. Concr. Inst. 68 (2) (1971) 126–135.
[2] P.S. Mangat, Tensile strength of steel fiber reinforced concrete, Cem. Concr. Res. 6 (2) (1976) 245–252.
[3] D.J. Hannant, Fiber Cements and Fibre Concrete, John Wiley and Sons Ltd., Chichester, 1978 219 pp.
[4] D.A. Fanella, A.E. Naaman, Stress–strain properties of fiber reinforced mortar in compression, ACI J. 82 (4) (1985) 475–483.
[5] A.S. Ezeldin, P.N. Balaguru, Normal- and high-strength fiber-reinforced concrete under compression, J. Mater. Civ. Eng. 4 (4) (1992) 415–429.
[6] G. Jianming, S. Wei, M. Keiji, Mechanical properties of steel fiber-reinforced, high-strength, lightweight concrete, Cem. Concr. Compos. 19 (4) (1997) 307–313.

[7] M.C. Nataraja, N. Dhang, A.P. Gupta, Stress–strain curve for steel-fiber reinforced concrete under compression, Cem. Concr. Compos. 21 (5) (1999) 383–390.
[8] P.S. Song, S. Hwang, Mechanical properties of high-strength steel fiber-reinforced concrete, Constr. Build. Mater. 18 (9) (2004) 669–673.
[9] S. Yazici, G. Inan, V. Tabak, Effect of aspect ratio and volume fraction of steel fiber on the mechanical properties of SFRC, Constr. Build. Mater. 21 (6) (2007) 1250–1253.
[10] J. Morton, G.W. Groves, The cracking of composites consisting of discontinuous reinforced concrete, J. Mater. Sci. 9 (9) (1974) 1436–1445.
[11] A.M. Brandt, On the optimal direction of short metal fibres in brittle matrix components, J. Mater. Sci. 20 (1985) 3831–3841.
[12] C.R. Chiang, A statistical theory of the tensile strength of short-fiber-reinforced composites, Compos. Sci. Technol. 50 (4) (1994) 479–482.
[13] N. Ozyurt, T.O. Mason, S.P. Shah, Correlation of fiber dispersion, rheology and mechanical performance of FRCs, Cem. Concr. Compos. 29 (2) (2007) 70–79.
[14] J.K. Kim, J.S. Kim, G.J. Ha, Y.Y. Kim, Tensile and fiber dispersion performance of ECC (Engineered Cementitious Composites) produced with ground granulated blast furnace slag, Cem. Concr. Res. 37 (7) (2007) 1096–1105.
[15] V.C. Li, Y. Wang, S. Backer, A micromechanical model of tension-softening and bridging toughness of short random fiber reinforced brittle matrix composites, J. Mech. Phys. Solids 39 (5) (1991) 607–625.
[16] S.Y. Fu, B. Lauke, Effect of fiber length and fiber orientation distributions on the tensile strength of short-fiber-reinforcement polymers, Compos. Sci. Technol. 56 (10) (1996) 1179–1190.
[17] I. Markovic, J.C. Walraven, J.G.M. van Mier, Self-compacting hybrid-fibre concrete — mix design, workability and mechanical properties, Proceedings of the Third International RILEM Symposium on Self-Compacting Concrete, Reykjavik, Iceland, 2003, pp. 763–775.
[18] P. Stähli, J.G.M. van Mier, Manufacturing, fibre anisotropy and fracture of hybrid fibre concrete, Eng. Fract. Mech. 74 (1–2) (2007) 223–242.
[19] P. Stähli, M. Sutter, J.G.M. van Mier, Improving the mechanical properties of HFC by adjusting the filling method, Proceedings of the Fifth International RILEM Workshop on High Performance Fiber Reinforced Cement Composites (HPFRCC5), Mainz, Germany, 2007, pp. 23–30.
[20] A. Poitou, F. Chinesta, G. Bernier, Orienting fibers by extrusion in reinforced reactive powder concrete, J. Eng. Mech. 127 (6) (2001) 593–598.
[21] S.T. Kang, J.J. Park, G.S. Ryu, S.W. Kim, Investigation of fiber alignment of UHSFRC in flexural members, Proceedings of 8th International Symposium on Utilization of High-strength and High-performance Concrete, Tokyo, Japan, 2008, pp. 709–714.
[22] J. Wuest, E. Denarié, E. Brühwiler, L. Tamarit, M. Kocher, E. Galluci, Determination of fibre distribution and orientation in fibre reinforced composites, Exp. Tech. 33 (5) (2009) 50–55.
[23] J. Wuest, E. Denarié, E. Brühwiler, Measurement and modelling of fibre distribution an d orientation in UHPFRC, Proceedings of the Fifth International RILEM Workshop on High Performance Fiber Reinforced Cement Composites (HPFRCC5), Mainz, Germany, 2007, pp. 259–266.
[24] J. Wuest, E. Denarié, E. Brühwiler, Model for predicting the UHPFRC tensile hardening response, Proceedings of the Second International Symposium on Ultra High Performance Concrete, Kassel, Germany, 2008, pp. 153–160.
[25] H.L. Cox, The elasticity and strength of paper and other fibrous materials, Br. J. Appl. Phys. 3 (3) (1952) 72–79.
[26] A. Bentur, S. Mindess, Fibre Reinforced Cementitious Composites, Elsevier Science Publishing Co., Inc., 1990 38 pp.
[27] M.R. Piggott, Load bearing Fibre Composites, Pergamon Press, Oxford, 1980 277 pp.
[28] V. Laws, The efficiency of fibrous reinforcement of brittle matrices, J. Phys. D: Appl. Phys. 4 (11) (1971) 1737–1746.
[29] M.R. Piggott, Short fibre polymer composites: a fracture-based theory of fibre reinforcement, J. Compos. Mater. 28 (7) (1994) 588–606.
[30] Y. Lee, S.T. Kang, J.K. Kim, Pullout behavior of inclined steel fiber in an ultra-high strength cementitious matrix, Constr. Build. Mater. 24 (10) (2010) 2030–2041.
[31] I. Markovic, High-performance hybrid-fiber concrete-development and utilisation. Delft University of Technology, Doctorial Thesis, Netherland, 2006, pp. 50–57.
[32] CEB-FIP, CEB-FIP Model Code 1990, Thomas Telford, London, 1993.
[33] P. Richard, M. Cheyrezy, Composition of reactive powder concretes, Cem. Concr. Res. 25 (7) (1995) 1501–1511.
[34] T. Kanakubo, K. Shimizu, M. Katagiri, T. Kanda, H. Fukuyama, K. Rokugo, Tensile characteristics evaluation of DFRCC — round robin test results by JCI-TC, Proceedings of International Workshop on HPFRCC in Structural Applications, Honolulu, USA, 2005, pp. 27–36.
[35] K. Rokugo, Tension tests and structural applications of strain-hardening fiber-reinforced cementitious composites, Proceedings of FraMCoS-7, Jeju, Korea, 2010, pp. 1533–1540.
[36] B.Y. Lee, Fiber distribution evaluation using digital image processing and its effect on tensile behavior of fiber reinforced cement composites. Korea Advanced Institute of Science and Technology, Doctorial Thesis, Korea, 2009, pp. 5–43.
[37] K. Kobayashi, Fiber Reinforced Concrete, Ohm-sha, Tokyo, 1981.